PLGA-PEG nanoparticles for targeted delivery of the mTOR/PI3kinase inhibitor dactolisib to inflamed endothelium

Gholizadeh, Shima; Kamps, Jan A A M; Hennink, Wim E; Kok, Robbert J

Published in:
International Journal of Pharmaceutics

DOI:
10.1016/j.ijpharm.2017.10.032

Publication date:
2018

International Journal of Pharmaceutics 548 (2018) 747–758

Contents lists available at ScienceDirect

International Journal of Pharmaceutics

journal homepage: www.elsevier.com/locate/ijpharm

PLGA-PEG nanoparticles for targeted delivery of the mTOR/PI3kinase inhibitor dactolisib to inflamed endothelium

Shima Gholizadeh[a], Jan. A.A.M. Kamps[b], Wim E. Hennink[a], Robbert J. Kok[a,*]

[a] Department of Pharmaceutics, Utrecht Institute for Pharmaceutical Sciences, Utrecht University, Utrecht, The Netherlands
[b] Department of Pathology & Medical Biology, Medical Biology Section, University Medical Center Groningen, University of Groningen, Groningen, The Netherlands

ARTICLE INFO

Keywords:
Targeted delivery
PLGA
NVP-BEZ235
Nanoparticles
Inflammation

ABSTRACT

Dactolisib (NVP-BEZ235, also referred to as: 'BEZ235' or 'BEZ') is a dual mTOR/PI3 K inhibitor that is of potential interest in the treatment of inflammatory disorders. This work focuses on formulation of BEZ-loaded polymeric nanoparticles composed of a blend of poly(D,L-lactide-co-glycolide) (PLGA) and poly(D,L-lactide-co-glycolide)-poly(ethylene glycol)-2000 (PLGA-PEG). The nanoparticles were prepared by an oil/water emulsion solvent evaporation method, and were subsequently characterized for yield, encapsulation efficiency, morphology, particle size, drug-polymer interaction and *in vitro* drug release profiles. A targeted formulation was developed by conjugation of a S-acetyl-thioacetyl (SATA)-modified mouse-anti human E-selectin antibody to the distal end of PLGA-PEG-SPDP containing nanoparticles. Our results show the successful preparation of spherical PLGA/PLGA-PEG nanoparticles loaded with BEZ. The particle size distribution showed a range from 250 to 360 nm with a high (> 75%) BEZ encapsulation efficiency. Approximately 35% of the loaded BEZ was released within 10 days at 37 °C in a medium containing 5% bovine serum albumin (BSA). Evaluation of efficacy of anti-E-selectin decorated BEZ-loaded nanoparticles was carried out in tumor necrosis factor-α (TNF-α) activated endothelial cells. Confocal microscopy analysis showed that cellular uptake of the targeted nanoparticles and subsequent internalization. Cell functional assays, including migration assay and phosphowestern blot analysis of the mTOR and pI3K signaling pathways, revealed that the E-selectin targeted nanoparticles loaded with BEZ had a pronounced effect on inflammation-activated endothelial cells as compared to the non-targeted BEZ-loaded nanoparticles. In conclusion, E-selectin targeted nanoparticles have a high potential in delivering the potent mTOR/pI3K inhibitor dactolisib to inflamed endothelial cells and are an interesting nanomedicine for anti-inflammatory therapy.

1. Introduction

In many inflammatory disorders endothelial cells are the key players in induction and progression of the disease (Pober and Sessa, 2007). Activation of this cell type by pro-inflammatory cytokines induces deregulation of various signaling pathways resulting in recruitment of inflammatory cells and induction of fibrotic pathways (Arango Duque and Descoteaux, 2014; Grivennikov et al., 2010; Karar and Maity, 2011). One of these pathways is the PI3K/AKT/mTOR signaling cascade, deregulation of which causes proliferation, malfunctioning and morphological changes of endothelial cells (ECs), cumulating in fibrotic tissue formation as a long term consequence (Karar and Maity, 2011; Maeshima and Makino, 2010; Fokas et al., 2012; Liu et al., 2009a). It is important to note that the PI3K pathway is involved in many different cellular functions under normal physiological conditions, including cell growth and proliferation, inhibition of apoptosis, cell metabolism, and intracellular signal transduction (Engelman et al., 2006). Many of these functions occur as a result of PI3K's interplay with its downstream effectors, Akt and mTOR, the latter being a kinase that is involved in the regulation of cell growth, angiogenesis, and metabolism (Dy and Adjei, 2009)

Small molecular inhibitors of intracellular signaling kinases are under investigation as chemotherapeutics for anti-inflammatory treatment (Dinarello, 2010). However, many intracellular signaling molecules are involved in cellular functions both under normal and under pathological conditions. Recent studies have shown that inhibition of activated PI3K/Akt and mTOR signaling in inflamed endothelial cells resulted in diminished immune responses by suppressing the secretion of pro-inflammatory cytokines (Fokas et al., 2012; Bhatt et al., 2010; Liang et al., 2014)

Dactolisib (referred to as NVP-BEZ235 or BEZ in the rest of this article) is a synthetic imidazoquinoline derivative with a hydrophobic

* Corresponding author at: Department of Pharmaceutics, Utrecht Institute for Pharmaceutical Sciences (UIPS), Universiteitsweg 99, 3584 CG Utrecht, The Netherlands.
E-mail address: r.j.kok@uu.nl (R.J. Kok).

http://dx.doi.org/10.1016/j.ijpharm.2017.10.032
Received 6 July 2017; Received in revised form 27 September 2017; Accepted 13 October 2017
Available online 16 October 2017

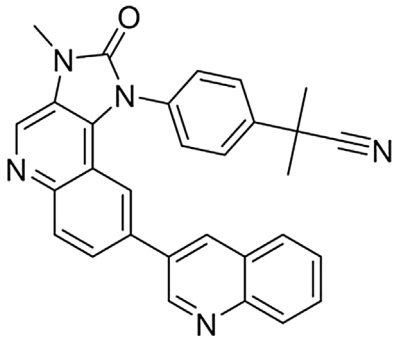

Scheme 1. Molecular structure of dactolisib (NVP-BEZ235). Mw: 469.6 g/mol; logP: 5.2 (PubChem).

character (Log P = 5.2) (Scheme 1). It is a drug candidate under phase I/II clinical trials as an anti-cancer therapeutic with a highly selective, reversible inhibitory effect on class I PI3K, and mTORC complexes (mTORC1 and mTORC2). (Maira et al., 2008; Baumann et al., 2009; Liu et al., 2009b; Bendell et al., 2015; Polivka and Janku, 2014). However, the clinical potential of BEZ is limited due to its low bioavailability after oral administration and pharmacokinetic variability among patients (Bendell et al., 2015; Burris et al., 2010). In order to increase the therapeutic efficacy and reduce side effects of (hydrophobic) drugs and drug candidates, various types of drug carrier systems have been developed over the past decade. Typical examples of such carrier systems are polymeric nanoparticles (NPs), (polymeric) micelles, and liposomes (Zhang et al., 2008; Farokhzad and Langer, 2009; Deng et al., 2012). Polymeric NPs in particular have attracted a lot of interest in recent years (Duncan and Gaspar, 2011; Kamaly et al., 2016). Based on the polymer composition they can be used to dissolve/encapsulate (hydrophobic) drug molecules and biotherapeutics (e.g. pharmaceutical proteins and nucleic acid based drugs), which enables enhanced circulation time in the bloodstream, sustained drug release, and (active) targeting to specific sites in the body (Duncan and Gaspar, 2011; Kamaly et al., 2016; Lammers et al., 2010). Poly(lactide-co glycolide) (PLGA) with and without a PEG block is frequently used for the design of drug carrier systems due to their good biocompatibility and biodegradability (Cho et al., 2013; Zhang et al., 2014; Anderson and Shive, 2012).

Nanoparticles with site-selective ligands bound to their surface have been shown to improve the desired site-selective drug delivery, while also increasing their active cellular uptake (Laquintana et al., 2014; Ambade et al., 2005). Out of the various types of targeting ligands (e.g. peptides, glycoproteins, carbohydrates, antibodies) that have thus far been used in targeted drug delivery, monoclonal antibodies (mAbs) are the most widely studied type of ligands (Van der Meel et al., 2013).

During inflammation the secretion of cytokines, such as tumor necrosis factor-α (TNF-α) and interleukin-1β (IL-1β), by immune cells induces an increase in the expression of several different adhesion molecules, such as E-selectin, vascular cell adhesion molecule-1 (VCAM-1), and intercellular adhesion molecule-1 (ICAM-1) on these endothelial cells (Sprague and Khalil, 2009). Of the above mentioned adhesion molecules, E-selectin in particular has been identified as a suitable adhesion molecule for drug or carrier system delivery to inflamed endothelial cells (Asgeirsdóttir et al., 2003; Jubeli et al., 2012).

The aim of the present study was to formulate PEGylated PLGA NPs loaded with the BEZ drug for active targeting of inflamed endothelial cells. First, various formulation parameters were evaluated to study their effects on the final characteristics such as size, morphology, BEZ encapsulation efficiency and release kinetics. Subsequently, selected NP formulations were surface functionalized with E-selectin antibody, in order to render them endothelial cell specific. The targeting (*i.e.* specific cell binding) capacity of such surface functionalized NPs was evaluated by comparing formulations with varying surface antibody densities. Finally, the intracellular uptake and efficacy of the targeted BEZ loaded NPs were assessed on E-selectin (over)expressing HUVEC cells by cell migration assay, as well as western blot analysis on the PI3K and mTOR signaling pathways.

2. Materials and methods

2.1. Materials

PLGA 5004A (molecular weight 20,000 Da), a copolymer of D,L-lactide and glycolide was obtained from Corbion Purac (Gorinchem, the Netherlands). Poly(ethylene glycol) monomethyl ether (molecular weight 2000 Da) was purchased from Sigma Aldrich (Germany). HO-PEG-NH_2 (Mw 2000 Da) was obtained from NOF corporations (Kyoto, Japan). Di-*tert*-butyl dicarbonate (Boc-o-Boc), poly(vinyl alcohol) (PVA; MW 13,000–23,000; 86–88% hydrolyzed), tin (II) 2-ethylhexanoate (SnOct2) and aldrithiol-2 were products of Sigma Aldrich. TNBSA (2,4,6-trinitrobenzene sulfonic acid) solution, succinimidyl 3-(2-pyridyldithio)propionate (SPDP), N-succinimidyl-S-acetylthioacetate (SATA) and rhodamine-NHS were obtained from Thermo scientific (Landsmeer, the Netherlands). Formaldehyde (4%) in PBS buffer was obtained from Fluka (Zwijndrecht, The Netherlands). NVP-BEZ235 was purchased from LC laboratories, USA. 4′,6-Diamidino-2-phenylindole (DAPI) was obtained from Roche (Penzberg, Germany). Phosphate buffer saline (PBS: NaCl 8.2 g, $Na_2HPO_4.12H_2O$ 3.1 g, $NaH_2PO_4.2H_2O$ 0.3 g in 1 l of water for injection, pH 7.4) was obtained from Braun (Melsungen AG, Germany). All other chemicals and reagents were obtained from Sigma Aldrich (Zwijndrecht, The Netherlands), unless otherwise mentioned.

2.2. Copolymer synthesis and preparation of nanoparticles

A PEG-PLGA copolymer was synthesized by ring opening polymerization of D,L-lactide (1.44 g, 0.01 mol) and glycolide (1.16 g, 0.01 mol) using H_3CO-PEG2000-OH (0.50 g, 0.25 mmol), and stannous octoate (0.05 g, 0.12 mmol) as initiator and catalyst, respectively. Details on the synthesis can be found in the Supplementary information. Nanoparticles (NPs) were prepared by a single emulsion solvent evaporation technique adapted from methods previously described by McCall et al. (McCall and Sirianni, 2013) with some modifications. In short, the polymers PLGA and PEG-PLGA in varying weight ratios of 100:0, 90:10, 80:20, 70:30, 50:50, 20:80, 0:100, were dissolved in chloroform to a final concentration of 5% w/v (0.10 g/2 ml). For BEZ loaded NPs, first a stock solution of BEZ in chloroform at concentration of 5 mg/ml was prepared. Next, 0.2, 1, or 2 ml of this solution were pipetted into vials containing 100 mg of blend polymers and volumed up to 2 ml with chloroform. Next, the obtained solutions were emulsified in an external aqueous phase (15 ml) containing poly(vinyl alcohol) 1% (w/v) in NaCl 0.9% (w/v) (filtered through a 0.2 μm Millipore filter), by an ultrasonic homogenizer (LABSONIC P, B. Braun Biotech) for 2 min at 45% amplitude to form an oil-in-water (o/w) emulsion. Chloroform was subsequently evaporated at 30 °C under reduced pressure for about 30 min, after which the resulting nanoparticle dispersion was kept under a nitrogen flow for 20 min at room temperature. The NPs were washed three times with 40 ml of PVA 1% (w/v) in NaCl 0.9% (w/v), by ultracentrifugation (J-26XP, Beckman Colter, Avanti) at 14000*g* for 10 min, followed by resuspension in demineralized water, ultracentrifugation, and resuspension in HBS buffer (containing 10 mM Hepes and 135 mM NaCl, pH 7.4). For freeze drying, the washed NPs were resuspended in demineralized water, aliquoted and lyophilized under vacuum (−49 °C and < 1 mHg) in a Chris Alpha 1–2 freeze-drier (Osterode am Harz, Germany) for 12 h.

Anti-E-selectin decorated NPs were prepared by incorporation of PLGA-PEG-SPDP (synthesized as described in Supporting information) at PLGA-PEG-SPDP to PLGA-PEG weight ratios of 100:0, 83:17, 50:50 and 0:100. Mouse anti-human E-selectin (IgG2a) was purified from the

supernatant of hybridoma H18/7 cells, kindly provided by Dr. M. Gimbrone Jr. (Harvard Medical School, Boston, MA) (Spragg et al., 1997), and modified with S-acetylthioacetyl (SATA) (8:1 SATA: Ab mol ratio) as described previously (Everts et al., 2003). Prior to coupling, the SATA-modified E-selectin antibody (2 mg/ml in HBS buffer) was treated with deacetylation buffer (consisting of 0.5 M Hepes, 0.5 M hydroxylamine–HCl, and 25 mM EDTA at pH 7.4) at 1/10 (v/v) for 45 min at room temperature (Oliveira et al., 2010), to deprotect the thioacetyl groups and to subsequently allow coupling with the SPDP end groups on the nanoparticle surface. The solution with activated antibody was added to the NP suspension at a concentration of 10 μg Ab/mg polymer, and incubated overnight at 4 °C. Prepared NPs were centrifuged and washed with HBS buffer (pH 7.4). Finally, the NPs were suspended in HBS buffer, pH 7.4. Negative control NP decorated with SATA-modified human serum IgG (Sigma Aldrich, Germany) were prepared with 0:100 wt ratio of PLGA-PEG to PLGA-PEG-SPDP.

Fluorescently labeled NPs were prepared by addition of 1 wt% of PLGA-PEG-rhodamine (synthesized as described in Supporting information) to the polymer mixtures.

Cell experiments were conducted with BEZ loaded NPs prepared using 9 wt% BEZ, 64 wt% PLGA and 27 wt% PLGA-PEG. The latter polymer was replaced by PLGA-PEG-SPDP when preparing the targeted formulation.

2.3. Nanoparticle characterization

2.3.1. Size and charge determinations

Freshly prepared NPs dispersions were diluted 100 times with 10 mM HEPES, pH 7.0 (final concentration 50 μg/ml). The size of the NPs was measured using dynamic light scattering (DLS, Malvern Instruments, Malvern, UK). The intensity-weighted average (z-average) and the polydispersity index (PDI) of the samples were determined by analyzing the correlation function (cumulants analysis) using Malvern software. The measurements were performed at 25 °C, at an angle of 90°. The ζ-potential of the nanoparticles was analyzed using Malvern Zetasizer Nano-Z (Malvern instruments) with disposable folded capillary cells. Nanoparticle (NP) dilutions were prepared as described in the previous paragraph. The zeta potential measurements were performed at 25 °C, and analyzed using DTS Nano 4.20 software. The morphology and size of the nanoparticles were studied by Transmission Electron Microscopy (TEM, Tecnai 10, Philips, 100 kV). Dilutions (100×) of nanoparticles (NPs) in HBS buffer (concentration 50 μg/ml) were prepared. Next, 25 μl of the NP suspension was pipetted onto parafilm, and a formvar/carbon-coated copper grid was placed on top of the sample droplet for 2 min to allow the particles to adsorb on the grid. Excess liquid was gently removed with a filter paper. The grid was negatively stained by placing it on top of a 20 μl droplet of 2% uranyl acetate in demineralized water supported on parafilm for 2 min. Excess liquid was gently removed by a filter paper and the grid was dried for 5 min at room temperature prior to the TEM analysis. Nanoparticles were visualized with 7–73k fold magnification and analyzed using MeasureIT software. TEM size estimates were calculated from 5 different areas on the grid. The total amount of particles analyzed for the TEM size estimates was 25 per sample.

2.3.2. Yield and drug loading of nanoparticles

Overall yield of nanoparticle preparation was determined by lyophilization of a 500 μl aliquot from the original nanoparticle (NP) dispersions (10 mg/ml) in demineralized water in pre-weighed Eppendorf tubes. The nanoparticle yield was calculated as percentage of the weight of the recovered product, divided by the total weights of polymers and drug that had been used to prepare the nanoparticles. Attachment or incorporation of PVA to the NPs was not considered in the calculations.

The BEZ loading efficiency was determined by dissolving a sample of lyophilized NPs in DMSO, of which a known aliquot was subsequently diluted further with acetonitrile and analyzed by UPLC. In detail, between 2 − 5 mg (accurately weighed) freeze-dried NPs was dissolved in 1 ml DMSO. Next, dilutions were made in acetonitrile (1/10 to 1/100), and samples were transferred into UPLC vials. Calibration was done by preparing serial dilutions in acetonitrile of a stock solution of BEZ in DMSO (concentration 1 mg/ml) in a concentration range of 0.05–100 μg/ml. An Acquity UPLC equipped with a BEH C18 1.7 μm column (2.1 × 50 mm) was used with a UV-detector (detection wavelength was 269 nm) for analysis. The gradient of the mobile phase (0.5 ml/min) was composed of 5% ACN in water with 0.05% TFA (solvent A) and 95% ACN in water with 0.05% of TFA (solvent B). Samples of 2 μl were injected.

BEZ encapsulation efficiency (EE) and loading capacity (LC) were calculated as follows:

$$EE = (\text{amount of measured BEZ/amount of BEZ added}) \times 100\%$$

$$LC = (\text{amount of measured BEZ})/\text{amount of (measured BEZ + polymer added)} \times 100\%$$

2.3.3. NMR measurements

The PEG-PLGA copolymers and the polymeric nanoparticles were characterized by ^{1}H NMR using a Gemini 300 MHz spectrometer (Varian Association Inc. USA). The copolymer composition, number-average molecule weight (M_n) and PEG content of the different copolymers, as well as the PEG incorporation efficiency in the polymeric particles, were determined by ^{1}H NMR after dissolution in DMSO-*d*6. Details on the ^{1}H NMR characterization of the copolymers and the nanoparticles can be found in the Supporting information.

2.3.4. Thermal analyses

The thermal behavior of formulated NPs was studied by differential scanning calorimetry, using a TA instruments DSC Q2000 machine. For polymers and freeze dried NPs, samples of 2 to 5 mg were accurately weighed and loaded into aluminum pans, which were subsequently closed. After equilibration at room temperature, the samples were heated to 100 °C (non-modulation) at a ramping rate of 2 °C/min under a nitrogen flow. Next, the samples were cooled down to −30 °C, modulated (± 1 °C every 30 s) at a ramping rate of 2 °C/min. Thereafter, the samples were heated to 100 °C modulated at a ramping rate of 2 °C/min. Two heating cycles were applied. The second heating cycle (modulated run) was used to determine the glass transition temperatures (T_g). Glass transition temperatures (T_g) are defined as the point of inflection of the step change observed in the heat flow curve.

2.3.5. Anti-E-selectin coupling efficiency

The antibody density on the surface of the NPs was determined using a micro-BCA protein assay kit (Pierce Biotechnology, Rockford, IL, USA) (Wiechelman et al., 1988). Calibration was performed using serial dilutions of mouse IgG (Sigma Aldrich, 0.16–50 μg/ml in HBS buffer). Coupling efficiency (CE%) is defined as the amount of Ab attached to NPs (measured with the micro-BCA assay) divided by the total amount of Ab added × 100%.

2.4. In vitro release of BEZ from nanoparticles

In vitro release experiments were conducted in HBS buffer (10 mM HEPES and 135 mM NaCl, pH 7.4) supplemented with BSA (50 mg/ml) to increase the solubility of released BEZ. Freshly prepared BEZ-loaded NPs were dispersed in incubation buffer in triplicate, and incubated at 37 °C under mild agitation. At different time points samples were taken, which were subsequently centrifuged at 22,000*g* for 10 min at 4 °C. The supernatant was collected for further analyses, and the pellets were resuspended in incubation buffer. The collected supernatants were treated in the following way: 50 μl of supernatant was taken per sample, to which 150 μl acetonitrile was added. Next, the samples were

vortexed for 10 s and kept at room temperature for about 1 h, followed by centrifugation for 10 min at 22,000*g* at 4 °C to spin down precipitated BSA. A sample of the supernatant was injected into the UPLC system for BEZ analysis as described above. The same pretreatment method was applied to BEZ standard solutions in incubation buffer in the concentration range of 0.4 to 200 μg/ml. Released BEZ was reported relative to the loaded amounts and fitted by different kinetic models (i.e. first order, zero order and Higuchi, assuming spherical particles) (Siepmann and Siepmann, 2012; Siepmann and Peppas, 2011).

BEZ release curves of the three different nanoparticle formulations were fitted with three different simple kinetic (drug-release) models:.

Zero order kinetics: $M_t = M_0 - k*t$; or: $-dM/dt = k$

First order kinetics: $M_t = M_0 * e^{k*t}$ (alternatively: $ln(M_t/M_0) = -k*t$); or: $-dM/dt = k*M_t$

Higuchi model (simplified): $M_t/M_0 = k*(t^{1/2})$

Where M_0 is the loaded amount of drug in the particles at time = 0, M_t is the amount of drug released from the particles at time = t, and k is the release rate constant. The three kinetic models each represent a fundamentally different type/mechanism of drug release from the polymeric NP formulations.

2.5. Experiments with endothelial cells

2.5.1. Binding of fluorescently labeled nanoparticles by flow cytometry

Human umbilical cord endothelial cells (HUVEC, Lonza) were seeded at 40,000 cells/well (96-well plates, Becton & Dickinson, Mountain View, CA, USA) and subsequently activated with TNF-α (10 ng/ml in EGM-2 medium) for 4 h at 37 °C (Kowalski et al., 2013). Fluorescently labeled NPs with varying surface antibody densities were diluted to concentrations of 0.1–8 mg polymer/ml in cell culture medium. The cells were incubated with the NPs for 1 h at 4 °C in the dark to avoid fluorochrome bleaching, after which they were washed three times with protein blocking agent (PBA) composed of 0.3% bovine serum albumin (BSA) in PBS. Finally, the cells were resuspended in 150 μl of PBA. The rhodamine fluorescence intensity of the different samples was determined using a BD FACSCanto (Becton & Dickinson). Typically, 10,000 events were acquired per sample prepared in triplicate. Data were analyzed using BD FACSDiva™ software (Becton & Dickinson) and results expressed as mean fluorescence intensity.

2.5.2. Binding and uptake of fluorescently labeled nanoparticles by confocal microscopy

HUVEC (30,000 cells) were seeded in FluoroDish (FD35-100, cell culture dish) and subsequently cultured overnight in full EGM-2 medium at 37 °C. Next, the cells were activated with 10 ng/ml of TNF-α for 4 h at 37 °C, followed by incubation of the cells with fluorescently labeled targeted and non-targeted nanoparticles (NPs), at a concentration of 100 μg/ml polymer, for 3 h at 37 °C. Following incubation, the cells were detached with trypsin/EDTA (Visweswaran et al., 2015), washed with plain medium, and the cells were then re-seeded in the FluoroDish plate. The cells were subsequently incubated for 1 h at 37 °C to allow their attachment on the plate surface. Next, the medium was removed and the cells were washed with PBS after which they were fixed with 4% formaldehyde in PBS for 30 min at room temperature. For nuclear staining, the cells were washed and incubated with DAPI at a concentration of 1 μg/ml for 5 min at room temperature. After three washing cycles, the petri dishes were dried and covered with FluorSave mounting agent (Calbiochem, San Diego, CA, USA) and kept at 4 °C for confocal analyses. The cellular uptake of NPs was visualized by a Z-axis scan of the sample using a Leica TCS-SP confocal laser-scanning microscope (Leica, Heidelberg, Germany) equipped with three lasers: 488 nm argon, 568 nm krypton, and 647 nm helium-neon. Scans were performed using steps of 0.8 μm. The cells were visualized at 3 to 4 μm Z-steps.

2.5.3. Effects of BEZ loaded nanoparticles in wound healing assay

HUVEC cells were seeded in 12 well plates at a density of 40,000 cells per well in full EGM-2 medium and cultured for 24 h at 37 °C. Next, the cells were incubated with TNFα (10 ng/ml) for 4 h at 37 °C and subsequently dispersions of targeted BEZ loaded and control NPs as well as solution of free BEZ at concentrations of 10 and 50 nM were added to the cells and incubated for 12 h at 37 °C. Subsequently, a scratch was introduced in the cell monolayer using a p200 pipet tip with diameter of 1.8 mm. Thereafter, the cells were washed with PBS followed by the addition of plain medium (without TNFα). The wound area was checked at time 0 (the moment of introducing scratch) and after 16 h incubation of the cells with plain medium at 37 °C. The wound surface area was analyzed using NIH Image J software. Wound closure was quantified by calculating the scratch wound area relative to surface area at t = 0.

2.5.4. Effects of BEZ loaded nanoparticles on mTOR and Pi3K signaling cascades

HUVEC cells were seeded in 6 well plates at a density of 100,000 cells/well and allowed to adhere overnight, followed by activation with TNF-α at concentration of 10 ng/ml for 4 h at 37 °C. Subsequently, control and targeted NPs loaded with BEZ as well as free BEZ were added to the cells at concentrations of 10 and 50 nM. The cells were incubated for 16 h at 37 °C, followed by washing with cold PBS and subsequent lysis with radio immune precipitation assay buffer (RIPA), supplemented with phosphatase/kinase inhibitor cocktail (Thermo Fisher Scientific, Rockford, IL, USA) on ice for 30 min. The lysates were centrifuged at 4 °C for 15 min at 14,000*g* and the obtained supernatants were stored at −20 °C. The protein concentration of the samples was determined using the micro-BCA assay. The supernatants were subjected to SDS-PAGE analysis using 4–12% gradient NuPAGE Novex Bis-Tris mini-gels (Invitrogen, Breda, The Netherlands). Proteins were electro-transferred onto a nitrocellulose membrane via iBlot Dry Blotting system. The membranes were blocked with 5% BSA in Tris-Buffered Saline containing 0.1% Tween-20 (TBS-T) for 2 h at room temperature. The membranes were stained overnight at 4 °C with rabbit monoclonal antibody against S6 Ribosomal protein (5G10), phospho-S6 ribosomal protein (Ser240/244) (D68F8)XP, Akt (pan) (C67E7), *p*-Akt (S473) XP, P-PI3 K p85(Y458)/p55(Y199) and rabbit polyclonal antibody against β-actin (Cell Signaling Technology, Inc., Danvers, MA, USA). The antibodies were diluted 1:1000 (according to the manufactures protocol) in 5% BSA in TBS-T. After washing with TBS-T, the membranes were incubated for 2 h at room temperature with goat anti-rabbit horseradish peroxidase (HRP) conjugated secondary antibody (Cell Signaling Technology, Inc.), diluted 1:1000 in 5% BSA in TBS-T. The proteins were visualized and detected using supersignal west femto chemiluminescent substrate (Thermo Fischer Scientific) and a Gel Doc imaging system equipped with a XRS camera and Quantity one analysis software (Bio-Rad).

2.6. Statistical analysis

Statistical analysis of the data was performed by unpaired Student's *t*-test and one-way ANOVA. Values are represented as mean ± SD. Differences were considered significant at $p < 0.05$. Data were analyzed with Graphpad prism (Graphpad software 5.0b, San Diego CA, USA).

3. Results and discussion

3.1. Characteristics of placebo PLGA/PLGA-PEG nanoparticles

Placebo (i.e. drug free) NPs were prepared by a single emulsion-solvent evaporation method using different blend ratios of PLGA and

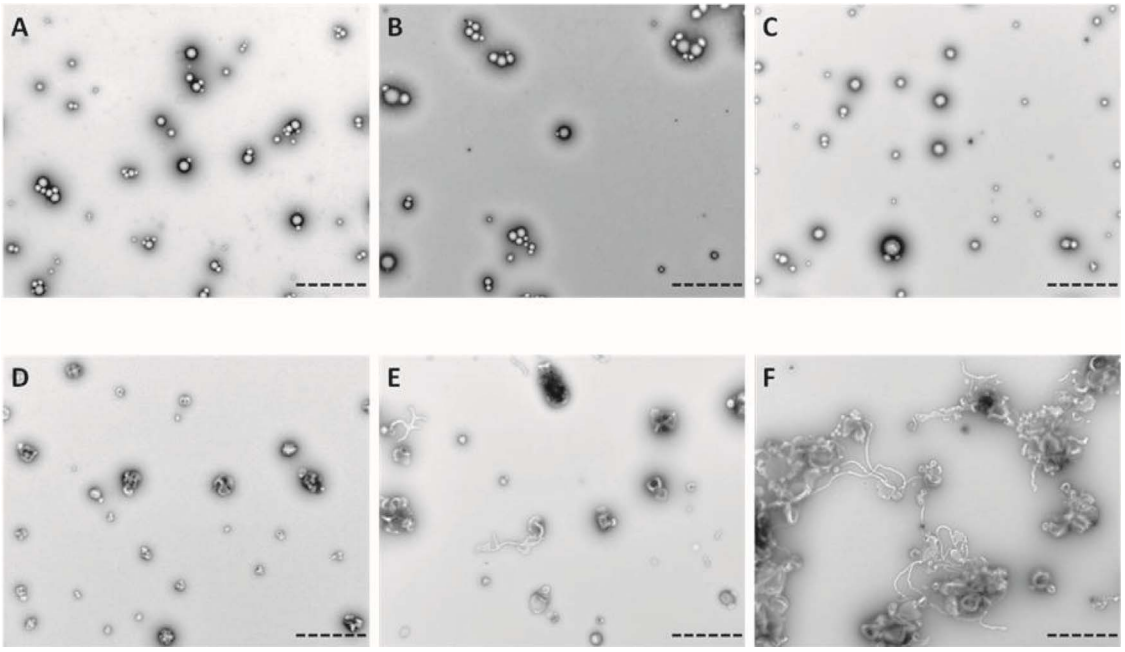

Fig. 1. TEM images of NPs with different wt% of PLGA-PEG in the formulation ranging from 0 to 100%. (A) with 0 wt% PLGA-PEG (B) 10 wt% of PLGA-PEG (C) 30 wt% of PLGA-PEG (D) 50 wt% of PLGA-PEG (E) 80 wt% of PLGA-PEG (F) 100 wt% of PLGA-PEG. Scale bar represents 2 μm.

Table 1
Characteristics of NPs formulated at 30 wt

# Formulation	TLC[a] (%)	DLS		Zeta Potential (mV)	Yield (%)	EE[b] (%)	DLC[c] (%)	T_g (°C)[d]	T_g (°C)[e]
		Size (nm)	PDI						
1	1.0%	317 ± 5	0.12 ± 0.05	−9.0 ± 0.3	71 ± 4	88.1 ± 3.4	0.87 ± 0.03	41.4	41.5
2	4.8%	290 ± 12	0.11 ± 0.03	−8.0 ± 0.2	75 ± 3	82.5 ± 3.7	4.0 ± 0.3	40.8	43.2
3	9.1%	342 ± 34	0.15 ± 0.02	−9.0 ± 0.5	72 ± 3	88.6 ± 5.9	8.1 ± 0.5	40.4	45.2

Data are presented as mean values ± SD for 3 preparations.

[a] Theoretical drug loading content.

[b] Encapsulation efficiency of the drug compound, as calculated from experimental/theoretical loading content DLC/TLC.

[c] Experimental drug loading content.

[d] Measured by DSC.

[e] Predicted by Gordon-Taylor equation: $T_g = (W_1Tg_1 + KW_2Tg_2)/(W_1 + KW_2)$ (Van den Mooter et al., 2001), in which W_1 and W_2 are the weight fractions of polymer and BEZ and $T_{g,1}$ and $T_{g,2}$ are the glass transition temperatures of the polymer and BEZ respectively, while K is defined as the ratio of the differences in expansion coefficient ($\Delta\alpha$) at T_g of the drug and the polymer (Gordon and Taylor, 1952). The measured T_g of the non-loaded NPs with a similar polymeric blend was 41.2 °C.

PLGA-PEG. NPs containing less than 30 wt% of PLGA-PEG had comparable characteristics in terms of size, with a particle diameter as determined by DLS analysis between 250 and 360 nm (Table S3). TEM analysis (Fig. 1) showed that NPs were spherical, with particle size ranging between 150- 200 nm. The nanoparticles had a negative zeta potential ranging between −11 to −15 mV (Table S3), while no significant differences in zeta potential were observed between the various PLGA-PEG wt% contents in the NP formulations. NPs prepared with 50 wt% or more PLGA-PEG had a clearly different morphology, with worm like structures being formed, in contrast to the spherical NPs that were formed at PLGA-PEG contents below 30 wt% (Fig. 1). Previously reported mechanistic studies on polymeric particle shape transformation have highlighted two main factors influencing the shape transformation kinetics of polymeric NPs. These are: 1) The viscoelastic properties of the applied polymer solutions, and 2) the interfacial tension between the polymer(-blocks) and the surrounding (aqueous-)medium (Williford et al., 2014; Chien et al., 2010; Blanazs et al., 2009). However, the exact interplay between these factors is highly complex, and the exact nature of these polymeric particle shape transformations would require a detailed investigation that is outside the scope of the present study. In subsequent experiments, we therefore further focused on NPs formulations that contained 30 wt% of PLGA-PEG.

Analysis of the various nanoparticles by ^{1}H NMR spectroscopy (Fig. S5) showed that within the experimental error PLGA-PEG was quantitatively incorporated in the formulation (Table S3, 64–101%).

DSC analyses were performed in order to determine the glass transition temperatures (T_g) of the obtained polymeric NPs. The DSC results showed that an increase in PLGA-PEG weight fraction from 0 to 30% results in a decrease of T_g from 48.1 °C to 41.2 °C (Table S3). The fact that only a single glass transition temperature was observed (see Fig. S9) for the blend NPs demonstrates that the PEG and PLGA blocks are fully miscible in their solid state. These results are consistent with data reported in previous papers in which the miscibility of PLGA and PEG was demonstrated (Jackson et al., 2007; Samadi et al., 2014). The high miscibility of the PEG and PLGA blocks is further supported by comparing the value of the experimentally observed T_g values with the ones calculated by the Fox equation for a blend of miscible polymers (Table S3).

3.2. Characteristics of BEZ loaded PLGA/PLGA-PEG nanoparticles

Encapsulation efficiency of BEZ was high (80–90%) and independent of the drug/polymer ratio in the feed, resulting in NPs with measured drug loadings varying between 0.9% and 8.1% (Table 1). The

size of drug-loaded NPs ranged from 290 to 342 nm with a polydispersity index (PDI) between 0.11 and 0.15, and a negative zeta potential between −8 and −9 mV. These values are comparable to the sizes and charge of placebo (i.e. non-loaded) NPs as reported in Table S3. In order to gain insight into the physical state of BEZ in the NPs, XRD crystallography (supplemental information Fig. S6) was performed on the formulation with the highest drug load content (8.1%). BEZ as well as placebo NP formulations were also measured for reference purposes. The X-ray diffractogram of BEZ showed sharp diffraction peaks at 12, 17 and 20 ° 2θ, indicating high crystallinity. In contrast, the XRD patterns of both the placebo (i.e. drug free) and BEZ-loaded NP formulations did not show sharp diffraction peaks, which demonstrates that the drug-loaded NP formulations are either amorphous or contain only nanocrystalline domains that are below the XRD detection limits. To further investigate the physical state of BEZ and to check whether the drug is molecularly dissolved or dispersed in the polymer matrix, DSC analysis was performed. The DSC thermogram of BEZ showed a melting peak at $T_{m(onset)}$ = 278 °C, based on which its T_g was predicted to be around 85 °C, using the equation $T_g = 0.67T_m$ (Alzghoul et al., 2014), as no clear T_g for BEZ was detected in the thermogram. Since the (calculated) T_g of BEZ (~85 °C) is higher than that of the non-loaded blend NP (41.2 °C) it is expected that a molecular dispersion of BEZ in the polymer matrix would result in an increase in T_g. Table 1 shows T_g for drug-loaded NP which are similar to the T_g of empty NPs (41.2 °C, Table S3). It is therefore it is unlikely that BEZ is molecularly dissolved in the polymeric matrix.

3.3. In vitro release of BEZ from PLGA/PLGA-PEG nanoparticles

Fig. 2 shows the *in vitro* release of BEZ-loaded NPs 1–3 with different drug load contents (0.9%, 4.0% and 8.1% DLC, see also Table 1).

Approximately 90% of the total loaded BEZ was released by the NPs with a 0.9% BEZ load content over a period of 10 days. The NPs with 4.0% and 8.1% BEZ load content released respectively 70% and 30% of their total drug content in the same timeframe.

To further analyze the *in vitro* BEZ release data, shown in Fig. 2, and to gain more insight into the potential mechanism of drug release, the BEZ release curves of the three different nanoparticle formulations were fitted with three different simple kinetic (drug-release) models, each representing a different type/mechanism of drug release from the polymeric NP formulations (Supplementary information, Table S4). As is clear from the respective equation, zero order kinetics assumes a (drug-) release rate that is constant over time. In principle, this would be ideal in cases where a constant drug concentration in the release medium is required during the release period. Instead, first order kinetics assumes an exponential correlation between time and amount of drug released (i.e. high initial release rate, decaying over time). Finally, the Higuchi model has been developed specifically to describe the release of drug molecules from a homogeneous (e.g. polymer) matrix in which the drug is dispersed. More details on the kinetic models used in this work can be found in the review by Siepmann (Siepmann and Peppas, 2011). It should be noted that the models fit reasonably well (correlation coefficients (R^2) of > 0.92) with the exception of the zero-order model for formulation 1 with 0.9% drug load content (DLC). Out of the three kinetic models that were evaluated, the first-order model showed the best fit to the experimental drug release data from the formulation 1 with 0.9% DLC. For the formulation 2 with 4.0% DLC, both first-order and Higuchi release models are excellent approximations (R^2 > 0.99 for both models), while the release profile of the formulation 3 with 8.1% DLC is best fitted by the Higuchi model. It is important to note that the Higuchi model in its simplified form disregards the effect of degrading (polymer) matrices on the drug release rate. This assumption was previously shown to be valid for PLGA NPs, since the degradation of PLGA heteropolymers start at approximately 2–6 weeks under similar conditions (Zweers et al., 2004; Belbella et al., 1996; Español et al., 2016).

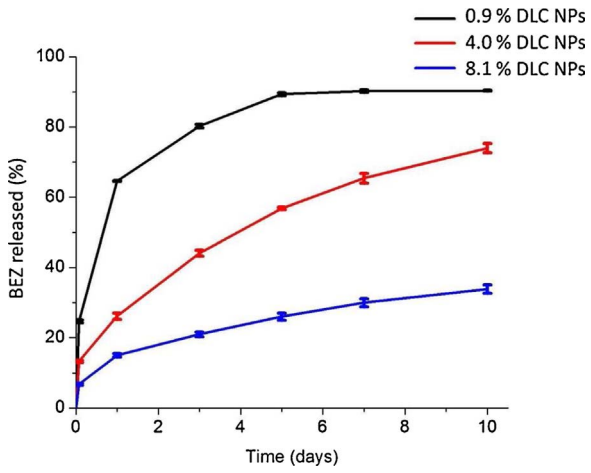

Fig. 2. *In vitro* release of BEZ from NP formulations #1–3 composed of 30 wt% of PLGA-PEG and varying weight percentages of BEZ. Release studies were performed at 37 °C in HBS buffer containing 5% BSA. Experimental DLC of formulations #1–3 are 0.9% w/w, 4.0% w/w and 8.1% w/w, respectively.

3.4. Characteristics of targeted placebo PLGA/PLGA-PEG NPs with different surface antibody densities

The characteristics of antibody-decorated NPs are summarized in Table 2. By varying the weight fraction of PLGA-PEG-SPDP in the NPs from 0 to 30 wt%, the Ab coupling efficiency increased from 2 to 37%. The size of the targeted NPs ranged from 260 to 360 nm with a PDI of 0.08 to 0.16, and the particles had a negative zeta potential ranging between −11 to −30 mV. The decrease in zeta potential (−11 to −30 mV) can be ascribed to an increase in antibody density on the surface of NPs, which can be explained by the negative charge of the anti-E-selectin monoclonal IgG Ab (pI: 5 to 6) at pH 7.4 (Agrisera Antibodies, 2017).

To calculate the Ab density per particle, the average particle diameter was taken as 200 nm (average value based on TEM, see Table S3), and the density of PLGA/PLGA-PEG NPs was taken as 1.3 g/cm^3 (Saha et al., 2014). As shown in Table 2 the Ab density for the NP formulation 7 was 95 Ab molecules per nanoparticle, while for formulations 6, 5 and 4, the Ab density decreased to 54, 14 and 5 Ab molecules per nanoparticle, respectively. These data indicate that the antibody molecules were mainly covalently attached (i.e. thiol linkage to the SPDP groups) to the surface of NPs, given the low a-specific adsorption of the antibody onto the NPs (i.e. 5 Ab/NP for particles without PLGA-PEG-SPDP).

3.5. Binding and uptake of fluorescently labeled nanoparticles by TNF-α activated HUVEC cells

Fig. 3 shows the binding of E-selectin targeted nanoparticles (NPs) to TNF-α activated endothelial cells as measured by flow cytometry analysis. The incubation time was fixed at 1 h and the temperature at 4 °C to exclude internalization. The results demonstrate that NPs in formulation 7 containing the highest antibody density (95 Ab/NP) on their surface had mean fluorescence intensity (i.e. cell-binding) values that were 3 times higher than the values of formulation 4 with the lowest Ab density (5 Ab/NP). The NPs with intermediate antibody densities (54 Ab/NP and 14 Ab/NP) showed binding levels that were in between the values of the NPs with the highest and the lowest antibody densities, while the mean fluorescence intensity of formulation 6 with a Ab density of 54 Ab/NP was clearly higher than that of formulation 5 with a Ab density of 14 Ab/NP. The negative control NPs (i.e. surface decorated with SATA modified IgG (non-specific) antibody) at the highest concentration, showed a binding comparable with formulation 4 having lowest (non-covalently bonded) antibody density (5 Ab/NP)

Table 2
Characteristics of targeted nanoparticle formulations.

# Formulation	NP Composition X:Y:Z[a]	NP Composition Ab: SPDP[b]	DLS		Zeta Potential (mV)	NP Yield (wt%)[c]	Ab coupled to NPs (wt%)[d]	Molecules Ab coupled/ nanoparticle[f]	Ab coupling efficiency (%)
			Size (nm)	PDI					
4	30: 0: 70	N.A.	256	0.13	−11.4	73	0.03[e]	5	2.0
5	25:05:70	9.2: 1	297	0.08	−17.0	75	0.07	14	5.2
6	15:15:70	3.1: 1	305	0.12	−24.9	72	0.27	54	19.4
7	0: 30: 70	1.5: 1	347	0.16	−30.5	81	0.46	95	37.0

[a] X:Y:Z = PLGA-PEG: PLGA-PEG-SPDP: PLGA5004A weight ratio in formulated nanoparticles (NP).
[b] Amount of antibody (Ab) added per formulation is constant at 1% of total polymer weight (=X + Y + Z). Calculated number is the theoretical antibody: SPDP-group weight ratio in the formulation.
[c] Percentage of total polymer weight (=X + Y + Z) in the formulation recovered as nanoparticles after washing steps.
[d] Calculated numbers are adjusted for NP yield.
[e] Physically adsorbed.
[f] Assuming NP density = 1.3 g/cm^3 and NP Ø = 200 nm, see main text.

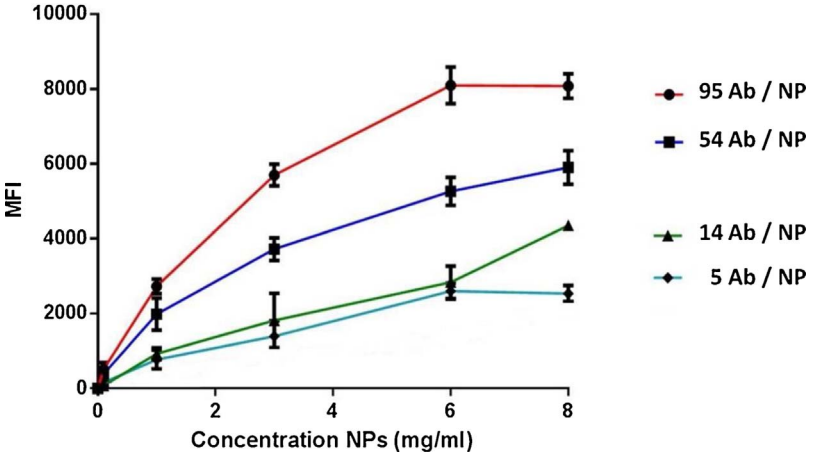

Fig. 3. FACS analysis of TNF-α activated HUVEC cells incubated with NPs formulations containing different Ab densities on their surface for a time period of 1 h at 4 °C in the presence of serum. Tested NP formulations are #4–#7 in Table 2 which have been decorated with different Ab/NP densities.

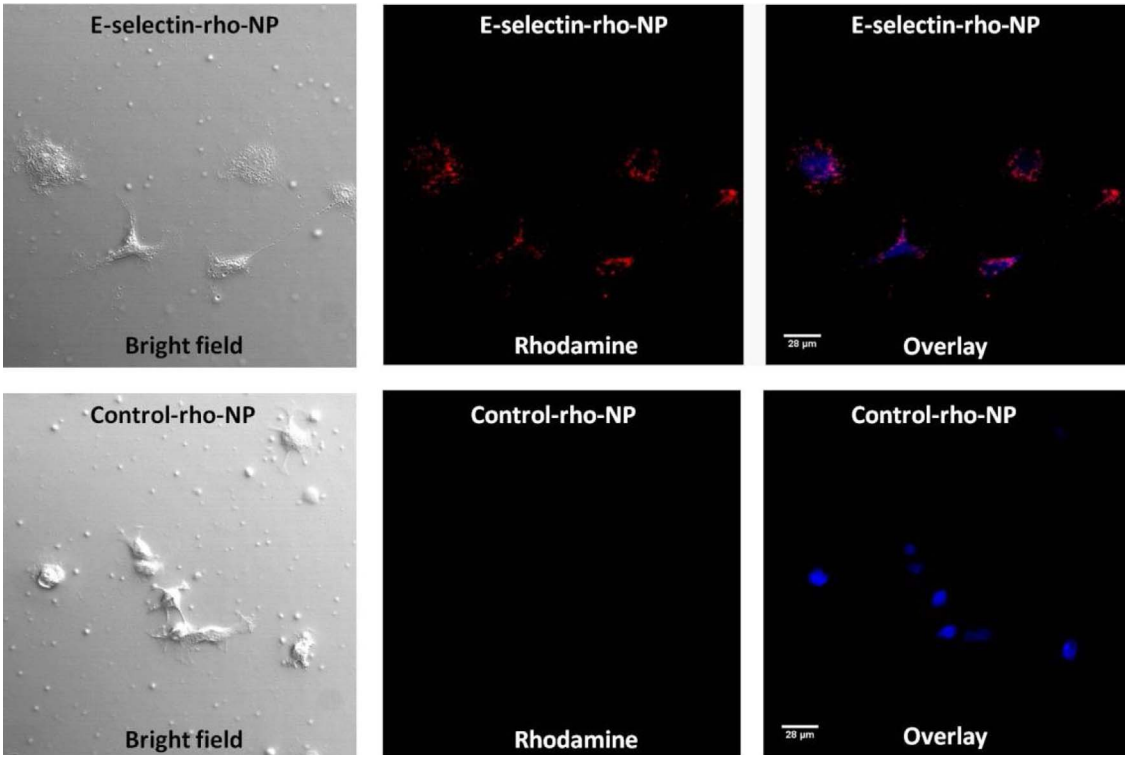

Fig. 4. Confocal laser scanning microscope (CLSM) images of activated HUVEC cells after incubation with targeted NPs (formulation #7)and control rhodamine labeled NPs in serum for 3 h at 37 °C. Scale bars in the figures represent 28 µm.

Table 3
Characteristics of targeted and control NPs loaded with BEZ.

# Formulation	Label	Size (nm)	PDI	Zeta Potential (mV)[a]	Yield[b] (%)	DLC (%)[c]	Drug loading efficiency (%)	Ab coupling efficiency (%)	Molecules Ab coupled/ nanoparticle
8	Targeted BEZ-loaded NPs	324 ± 40	0.20 ± 0.04	−20.8 ± 6.0	74 ± 7	6.7 ± 0.3	75 ± 4	36 ± 5	100 ± 22
9	Control BEZ-loaded NPs	313 ± 42	0.16 ± 0.07	−15.8 ± 4.6	73 ± 10	6.8 ± 0.5	78 ± 7	N.A.	N.A.

Presented data are the average of 3 preparations.
[a] Presented data are the average of 2 preparations.
[b] Yield is determined before Ab coupling to NPs.
[c] Experimental drug loading content.

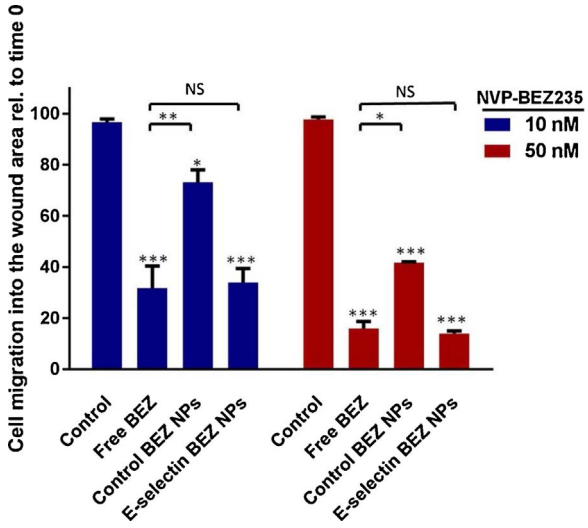

Fig. 5. Semi-quantitative analysis of closure of the scratch wound area, as calculated from the images taken at t = 0 h and t = 16 h. Data are plotted as mean values ± SEM of two individual experiments (n = 2) with the same formulations; *p < 0.05, **p < 0.01, ***p < 0.001 compared to TNF-α activated HUVEC cells (control), unless otherwise depicted. NS = not significant. Tested NP formulations are #8–9 in Table 3.

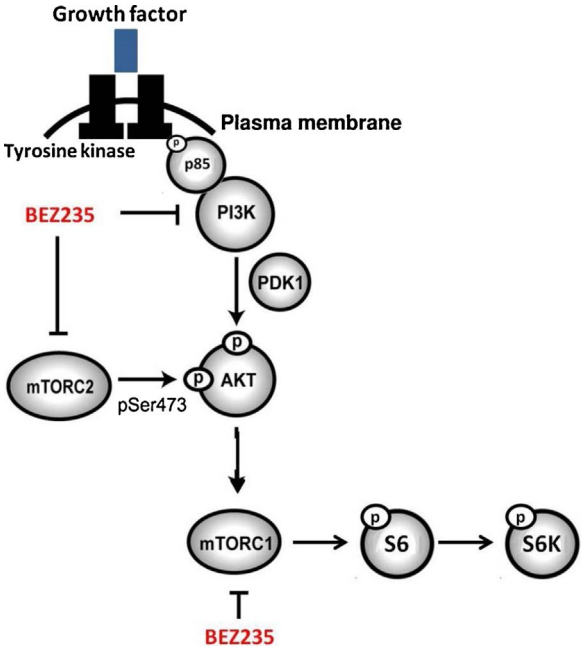

Scheme 2. Simplified representation of PI3 K/mTOR-related signaling and ATP-competitive dual PI3 K/mTOR inhibitor (i.e. BEZ235), which antagonize PI3 K and both mTOR complexes.
Adapted with permission from (Shortt et al., 2013). Copyright The American Society of Hematology.

(data not shown). These results show that the extent of NP cell binding correlates directly with the number of antibody molecules that are attached on their surface which is in agreement with previously reported findings (Gu et al., 2008). For further *in vitro* cell uptake and functionality assays, the formulation 7 composed of 70 wt% PLGA and 30 wt% of PLGA-PEG-SPDP was selected as targeted carrier system, focusing on the nanoparticle formulation with highest Ab density (95 Ab/NP).

The uptake of E-selectin targeted rhodamine labeled NPs by TNF-α activated HUVEC cells was visualized using confocal microscopy (Fig. 4). The cells were incubated with control PEG-PLGA NPs that had not been incubated with anti-E-selectin Ab and with targeted labeled NP with the highest density of anti-E-selectin Ab (formulation 7) for 3 h at 37 °C, to allow for receptor mediated internalization of the targeted NPs. The targeted uptake process resulted in a distinct increase in intensity of the rhodamine fluorescence pattern compared to the cells that were incubated with the non-targeted (control) NPs, as is shown in Fig. 4. These results suggest that targeted NPs are suitable carrier systems for active carrier system delivery to the cells.

3.6. Characteristics of BEZ loaded targeted and non-targeted (control) nanoparticles

Based on the results obtained from the previous sections regarding drug load content and antibody density on the surface of NPs, the final formulation to be tested for cell functional assays was composed of 70 wt% PLGA and 30 wt% PLGA-PEG-SPDP, functionalized with anti-E-selectin antibodies, and loaded with BEZ at 9.1% drug loading content (Table 3, formulation 8). Control (i.e. non-targeted) BEZ loaded NPs (formulation 9) were prepared with 30 wt% PLGA-PEG and had not been decorated with anti-E-selectin. Drug loading efficacies obtained for both formulations were high (approximately 75%), with Ab coupling efficiency being about 36% for the targeted formulation. DLS analyses showed that the mean hydrodynamic diameter of both types of NPs was approximately 300 nm. Of note, one can expect that the relatively large hydrodynamic size (i.e. ~300 nm) of formulated NPs in this study can be a limiting factor for future *in vivo* applications since it can activate the complement system and be quickly removed from the blood stream, accumulating in the liver and spleen. Optimizing the NP size is therefore a next logical next step before *in vivo* evaluation to confirm their capacity to effectively home to inflamed tissues. The targeted BEZ-loaded NPs showed a higher (negative) zeta potential value than the control BEZ-loaded NPs (-20.8 mV and −15.8 mV, respectively), which can be explained by the presence of negatively charged (at pH 7.4) antibody molecules (pI: 5–6) that are attached to the surface of the targeted NPs.

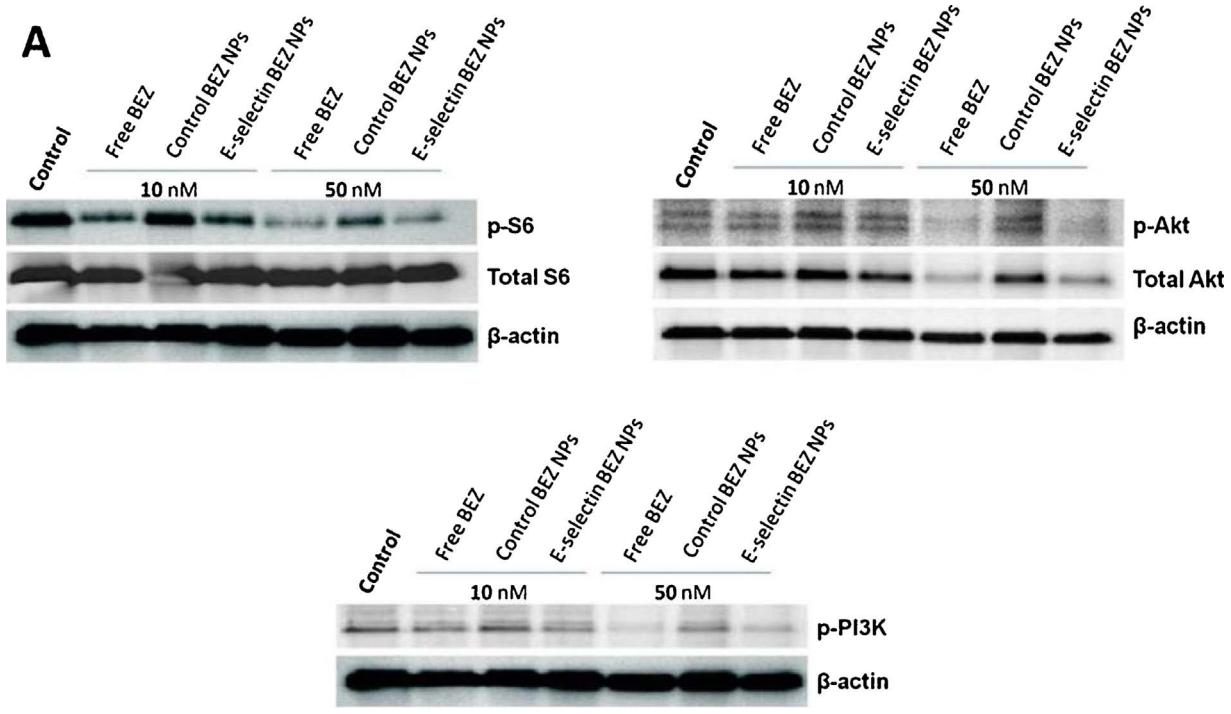

Fig. 6. Effect of BEZ and its NP formulations (at 10 nM and 50 nM BEZ concentrations) on total protein expression or phosphorylation levels in PI3 K and mTOR signaling pathways. Tested NP formulations are #8–#9 in Table 3. (A) Representative Western blot bands of phosphorylation of S6 protein (Ser 240/244), Akt (Ser 473), PI3K (Tyr 199/458) and total protein expression levels. β-actin expression was analyzed as a loading control. (B) Densitometry of Western blot bands in the blots. Results are normalized as ratio of protein expression level in treated cells compared to TNF-α activated HUVEC cells (control).

3.7. Pharmacological activity of targeted BEZ-loaded nanoparticles

3.7.1. Effects of targeted BEZ loaded nanoparticles in wound healing assay

The mTOR and PI3 K signaling cascades control a wide range of cellular responses, including cell motility and migration (Berven et al., 2004; Castellano et al., 2016). In previous studies it has been shown that TNF-α induced extracellular kinase signaling is involved in cell motility through Rho GTPase activity (Pollock et al., 2005; Vial et al., 2003). The PI3 K pathway is also involved in Rho family signal transduction which indirectly affects cell migration (Jiménez et al., 2000; Tolias et al., 1995).

To investigate the pharmacological characteristics of targeted NPs loaded with BEZ, the migration of endothelial cells was studied in a scratch wound healing assay with TNF-α activated HUVEC. Semi-quantitative analysis of the scratch wound area revealed that non-treated, TNF-α activated endothelial cells (i.e. control) repopulated the cell-free area for more than 95% in 16 h. Treatment with free BEZ reduced the closure of the scratch area in 16 h to values of approximately 30% and 15% at BEZ concentrations of 10 and 50 nM, respectively. BEZ loaded control (i.e. non-targeted) NPs also inhibited closure of the scratch wound area, although at a lesser extent compared to equivalent solutions of concentrations of free BEZ. Possible explanations for the observed effects of the control NPs can be either the non-specific cellular interaction of the (non-targeted) control NPs within the set exposure time, or (more likely) the release of BEZ from the control NPs into the surrounding medium during the incubation period. During 16 h of incubation the amount of BEZ released from the control NPs into the medium would be equal to approximately 10% of the total amount of BEZ present in the NP formulation, based on results discussed above in Section 3.3. A more important result from Fig. 5 is that the E-selectin targeted BEZ-loaded nanoparticles showed a strong reduction in cell migration, similar to the values achieved by free BEZ. The targeted formulations achieved a reduction of up to about 10% wound closure, corresponding to a 70% inhibition of cell migration at 10 nM BEZ concentrations and a 90% inhibition of cell migration at 50 nM BEZ concentrations (Fig. 5). Given that only 10% of the total drug loading is released from the NPs into the medium during the 16 h incubation period (see Fig. 2) the equal cellular effects observed for targeted BEZ-loaded nanoparticles and free BEZ point to a superior efficacy of the targeted formulation.

3.7.2. Effects of targeted BEZ loaded nanoparticles on PI3K and mTOR signaling cascades

In a similar setup as described above for cell migration, the effects of BEZ-loaded targeted NPs on the mTOR/PI3K signaling cascades were studied. BEZ has inhibitory effects on both the mTOR and PI3K signaling cascades (Kim et al., 2014). This can be visualized by determining the phosphorylation state of the downstream targets of these kinases, as shown in Scheme 2.

The direct effect of BEZ on the PI3K/mTOR signaling cascade was evaluated on total S6 ribosomal protein and its phosphorylated form at Ser240/244 residues, as well as on total Akt and its phosphorylated form at Ser473, while the indirect effect of the compound was analyzed on the phosphorylated form of PI3K at p85 (Tyr458)/p55 (Tyr199) via immunoblotting. The total S6, Akt and β-actin were used as a control to show that the BEZ treatment does not affect total amount of S6, Akt and β-actin proteins isolated from cell lysates.

Both free BEZ and E-selectin targeted BEZ-loaded NPs inhibited phosphorylation of the S6 ribosomal subunit at BEZ concentrations of 10 nM (Fig. 6A and B). The same figure also shows that at a BEZ concentration of 50 nM, the inhibitory effects for both treatments were more pronounced compared to the effects at a BEZ concentration of 10 nM.

The phosphorylation of Akt kinase also decreased upon treatment with free BEZ and E-selectin targeted BEZ-loaded NPs at BEZ concentrations of 10 and 50 nM (Fig. 6A and B). However, a decrease in total Akt level was also observed for both treatments, which can be attributed to the inhibitory effect of BEZ on PI3K/Akt signaling pathway (Kim et al., 2014).

Phosphorylation of the PI3K adaptor subunit (p85/p55) was

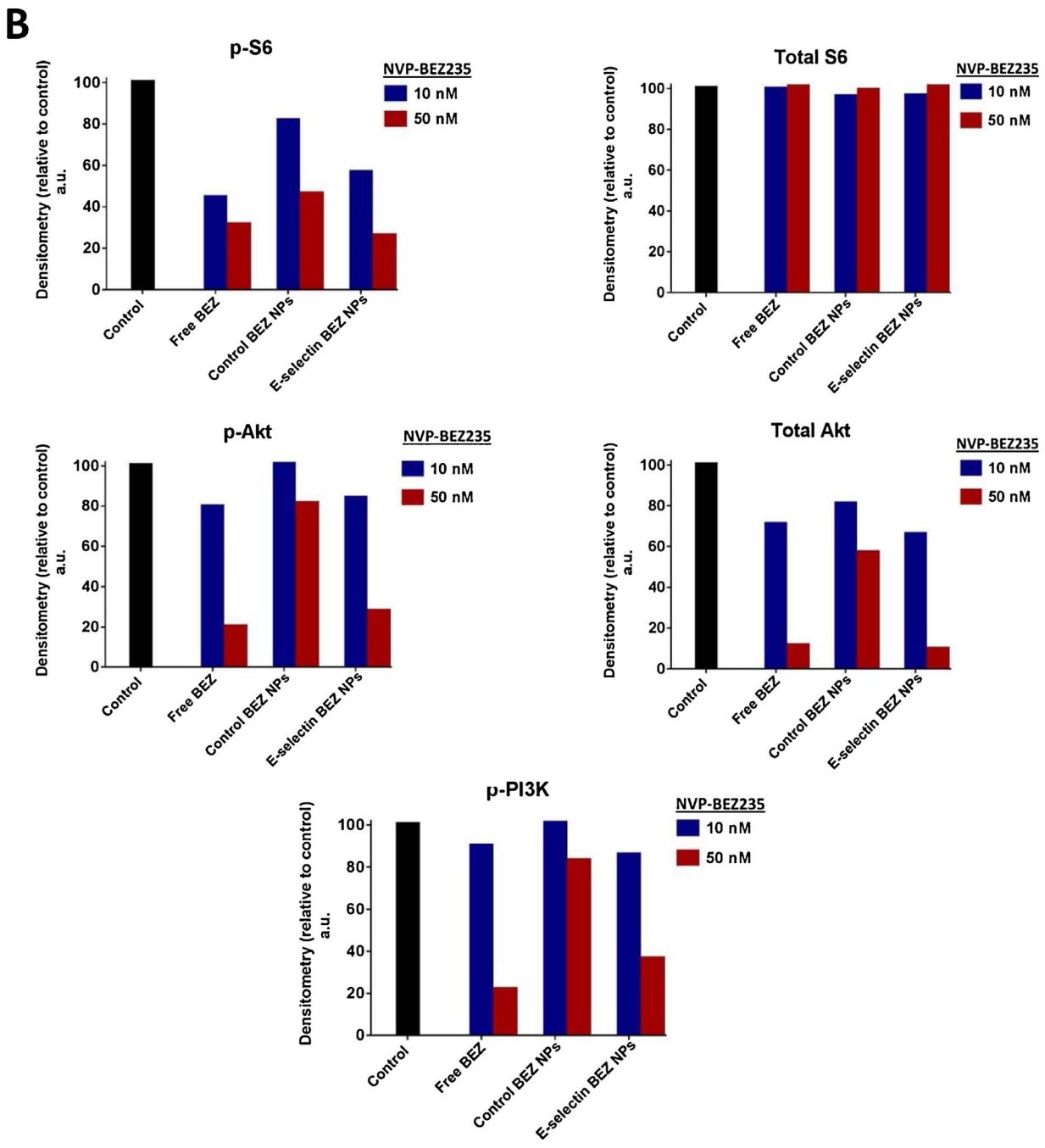

Fig. 6. (*continued*)

analyzed to confirm the indirect effect of the free BEZ and the BEZ-loaded NP formulations on the PI3K signaling pathway. Free BEZ and E-selectin targeted BEZ-loaded NPs at concentration of 10 nM and 50 nM indeed showed inhibition of phosphorylation of the PI3K adaptor subunit. In contrast, the control (*i.e.* non-targeted) BEZ-loaded NPs only showed (minor) inhibitory effects at the highest concentration of 50 nM (Fig. 6A and B).

The present data indicate that control (i.e. non-targeted) BEZ-loaded NPs did not achieve active intracellular BEZ delivery, and therefore failed to induce any significant inhibitory effect on cell migration and/or the PI3K/mTOR signaling cascade within the designated time period. On the other hand, the BEZ-loaded NPs that actively targeted E-selectin had an efficacy similar to that of the free BEZ, both concentrations of 10 nM and 50 nM. A similar trend was also observed in the cell migration assay discussed in the previous paragraph, confirming the efficient cellular uptake and subsequent cytoplasmic release of BEZ achieved by the targeted nanoparticles.

Although the initial *in vitro* results discussed in this work are promising, the question whether targeted BEZ-loaded NP formulations will be able to achieve an enhanced efficacy of BEZ *in vivo* still remains open. However, it is important to note that previously reported *in vivo* studies on E-selectin targeted nanomedicines (mainly liposome-based) have confirmed the high *in vivo* efficacy of the developed systems, as well as their capability to efficiently target the disease-affected endothelial cells that are primarily responsible for the inflammation (Asgeirsdóttir et al., 2008; Kowalski et al., 2014). Based on these promising *in vivo* results using targeted liposomal nanomedicines, the *in vitro* results of the E-selectin targeted BEZ-loaded NPs reported in this work can be viewed as a very encouraging starting point for future *in vivo* studies with targeted BEZ-loaded NP formulations.

It is important to note that the applied concentrations of 10 nM and 50 nM are above the half maximal inhibitory concentration (IC_{50}) (see Fig. S12). Based on the cell viability assay (MTS assay) about 80 to 90% cell viability was detected for the incubated cells in both the cell migration assay and the western blot analysis (see Fig. S13).

4. Conclusions

In this paper BEZ-loaded polymeric nanoparticles (NPs) are presented, which were used for delivery of a mTOR/PI3kinase inhibitor to TNF-α activated endothelial cells. The different BEZ-loaded NP formulations were composed of different ratios of PLGA and PLGA-PEG copolymers, where the PEG moiety of the latter was modified with an SPDP group to allow coupling of anti-E-selectin antibodies (Ab) when formulating targeted NPs. The nanoparticles were evaluated based on various characteristics, such as their particle size and morphology, BEZ loading, drug release kinetics, Ab coupling efficiency to NP surface, and the NP's ability to bind to activated endothelial cells. The most promising targeted BEZ-loaded nanoparticles were further tested *in vitro* using cell functionality assays, where they showed successful intracellular delivery and cytosolic release of the BEZ drug compound, achieving an efficacy that was comparable to the efficacy of an equivalent concentration of free BEZ. In contrast, the control (non-targeted) BEZ-loaded NPs showed an almost negligible efficacy, demonstrating that the targeting of E-selectin by functionalization of the NP surfaces with antibody molecules was critical to develop an effective BEZ nanocarrier.

Conflict of interest

The authors declare no conflict of interest.

Acknowledgements

This work has been supported by NanoNextNL, a micro and nanotechnology consortium of the government of The Netherlands and 130 partners (project 03D.07). The authors would like to thank Nazila Masoud (Utrecht University) for her assistance with the X-Ray diffraction measurements.

Appendix A. Supplementary data

Supplementary data associated with this article can be found, in the online version, at https://doi.org/10.1016/j.ijpharm.2017.10.032.

References

Agrisera Antibodies, 2017. Agrisera Antibodies, Molecular Weight and Isoelectric Point of Various Animal Immunoglobulins. (Accessed: June 1, 2017). http://www.agrisera.com/en/info/molecular-weight-and-isoelectric-point-of-various-immunoglobulins.html.

Alzghoul, A., Alhalaweh, A., Mahlin, D., Bergström, C.A., 2014. Experimental and computational prediction of glass transition temperature of drugs. J. Chem. Inf. Model. 54 (12), 3396–3403.

Ambade, A.V., Savariar, E.N., Thayumanavan, S., 2005. Dendrimeric micelles for controlled drug release and targeted delivery. Mol. Pharm. 2 (4), 264–272.

Anderson, J.M., Shive, M.S., 2012. Biodegradation and biocompatibility of PLA and PLGA microspheres. Adv. Drug Deliv. Rev. 64, 72–82.

Arango Duque, G., Descoteaux, A., 2014. Macrophage cytokines involvement in immunity and infectious diseases. Front. Immunol. 5 (491), 1–12.

Asgeirsdóttir, S.A., Kok, R.J., et al., 2003. Delivery of pharmacologically active dexamethasone into activated endothelial cells by dexamethasone-anti-E-selectin immunoconjugate. Biochem. Pharmacol. 65 (10), 1729–1739.

Asgeirsdóttir, S.A., Zwiers, P.J., Morselt, H.W., Moorlag, H.E., Bakker, H.I., Heeringa, P., Kok, J.W., Kallenberg, C.G., Molema, G., Kamps, J.A., 2008. Inhibition of proinflammatory genes in anti-GBM glomerulonephritis by targeted dexamethasone-loaded AbEsel liposomes. Am. J. Physiol. Renal Physiol. 294 (3), F554–61.

Baumann, P., Mandl-Weber, S., Oduncu, F., Schmidmaier, R., 2009. The novel orally bioavailable inhibitor of phosphoinositol-3-kinase and mammalian target of rapamycin, NVP-BEZ235, inhibits growth and proliferation in multiple myeloma. Exp. Cell Res. 315 (3), 485–497.

Belbella, A., Vauthier, C., Fessi, H., Devissaguet, J.-P., Puisieux, F., 1996. In vitro degradation of nanospheres from poly(D,Llactides) of different molecular weights and polydispersities. Int. J. Pharm. 129, 95–102.

Bendell, J.C., Kurkjian, C., Infante, J.R., et al., 2015. A phase 1 study of the sachet formulation of the oral dual PI3K/mTOR inhibitor BEZ235 given twice daily (BID) in patients with advanced solid tumors. Invest. New Drugs 33, 463–471.

Berven, L.A., Willard, F.S., Crouch, M.F., 2004. Role of the p70(S6K) pathway in regulating the actin cytoskeleton and cell migration. Exp. Cell Res. 296, 183–195.

Bhatt, A.P., Bhende, P.M., Sin, S.H., et al., 2010. Dual inhibition of PI3K and mTOR inhibits autocrine and paracrine proliferative loops in PI3K/Akt/mTOR-addicted lymphomas. Blood 115 (22), 4455–4463.

Blanazs, A., Armes, S.P., Ryan, A.J., 2009. Self-assembled block copolymer aggregates: from micelles to vesicles and their biological applications. Macromol. Rapid Commun. 30 (4–5), 267–277.

Burris, H., Rodon, J., Sharma, S., et al., 2010. First-in-human phase I study of the oral PI3K inhibitor BEZ235 in patients (pts) with advanced solid tumors. J. Clin. Oncol. 28 (Suppl. (15)) (abstr 3005).

Castellano, E., Molina-Arcas, M., Krygowska, A.A., East, P., Warne, P., Nicol, A., Downward, J., 2016. RAS signalling through PI3-kinase controls cell migration via modulation of Reelin expression. Nat. Commun. 7 (11245), 1–13.

Chien, M.P., Rush, A.M., et al., 2010. Programmable shape-shifting micelles. Angew. Chem. Int. Ed. Engl. 49 (30), 5076–5080.

Cho, E.J., Holback, H., Liu, K.C., Abouelmagd, S.A., Park, J., Yeo, Y., 2013. Nanoparticle characterization: state of the art, challenges, and emerging technologies. Mol. Pharm. 10 (6), 2093–2110.

Deng, C., Jiang, Y., Cheng, R., Meng, F., Zhong, Z., 2012. Biodegradable polymeric micelles for targeted and controlled anticancer drug delivery: promises, progress and prospects. Nanotoday 7 (5), 467–480.

Dinarello, C.A., 2010. Anti-inflammatory agents: present and future. Cell 140, 935–950.

Duncan, R., Gaspar, R., 2011. Nanomedicine(s) under the microscope. Mol. Pharm. 8 (6), 2101–2141.

Dy, G.K., Adjei, A.A., 2009. Emerging therapeutic targets in non-small cell lung cancer. Proc. Am. Thorac. Soc. 6, 218–223.

Engelman, J.A., Luo, J., Cantley, L.C., 2006. The evolution of phosphatidylinositol 3-kinases as regulators of growth and metabolism. Nat. Rev. Genet. 7, 606–619.

Español, L., Larrea, A., Andreu, V., Mendoza, G., Arruebo, M., Sebastian, V., Aurora-Prado, M.S., Kedor-Hackmann, E., Santoro, M.I., Santamaria, J., 2016. Dual encapsulation of hydrophobic and hydrophilic drugs in PLGA nanoparticles by a single-step method: drug delivery and cytotoxicity assays. RSC Adv. 6 (112), 1–11.

Everts, M., Koning, G.A., Kok, R.J., Asgeirsdóttir, S.A., Vestweber, D., Meijer, D.K., Storm, G., Molema, G., 2003. In vitro cellular handling and in vivo targeting of E-selectin-directed immunoconjugates and immunoliposomes used for drug delivery to inflamed endothelium. Pharm. Res. 20 (1), 64–72.

Farokhzad, O.C., Langer, R., 2009. Impact of nanotechnology on drug delivery. Acs Nano 3 (1), 16–20.

Fokas, E., Yoshimura, M., Prevo, R., et al., 2012. NVP-BEZ235 and NVP-BGT226: dual phosphatidylinositol 3-kinase/mammalian target of rapamycin inhibitors, enhance tumor and endothelial cell radiosensitivity. Radiat. Oncol. 7 (48), 1–13.

Gordon, M., Taylor, J.S., 1952. Ideal copolymers and the second-order transitions of synthetic rubbers: I. Non-crystalline copolymers. J. Appl. Chem. 2, 493–501.

Grivennikov, S.I., Greten, F.R., Karin, M., 2010. Immunity, inflammation, and cancer. Cell 140 (6), 883–899.

Gu, F., Zhang, L., Teply, B.A., Mann, N., Wang, A., Radovic-Moreno, A.F., Langer, R., Farokhzad, O.C., 2008. Precise engineering of targeted nanoparticles by using self-assembled biointegrated block copolymers. PNAS 105 (7), 2586–2591.

Jackson, J.K., Hung, T., Letchford, K., Burt, H.M., 2007. The characterization of paclitaxel-loaded microspheres manufactured from blends of poly(lactic-co-glycolic acid) (PLGA) and low molecular weight diblock copolymers. Int. J. Pharm. 342, 6–17.

Jiménez, C., Portela, R.A., Mellado, M., Rodríguez-Frade, J.M., Collard, J., Serrano, A., Martínez-A, C., Avila, J., Carrera, A.C., 2000. Role of the PI3K regulatory subunit in the control of actin organization and cell migration. J. Cell Biol. 151, 249–262.

Jubeli, E., Moine, L., Nicolas, V., Barratt, G., 2012. Preparation of E-selectin-targeting nanoparticles and preliminary in vitro evaluation. Int. J. Pharm. 426 (1–2), 291–301.

Kamaly, N., Yameen, B., et al., 2016. Degradable controlled-release polymers and polymeric nanoparticles: mechanisms of controlling drug release. Chem. Rev. 116, 2602–2663.

Karar, J., Maity, A., 2011. PI3K/AKT/mTOR pathway in angiogenesis. Front. Mol. Neurosci. 4 (51), 1–8.

Kim, K.W., Myers, C.J., Jung, D.K., Lu, B., 2014. NVP-BEZ-235 enhances radiosensitization via blockade of the PI3K/mTOR pathway in cisplatin-resistant non-small cell lung carcinoma. Genes Cancer 5, 7–8.

Kowalski, P.S., Lintermans, L.L., Morselt, H.W., Leus, N.G., Ruiters, M.H., Molema, G., Kamps, J.A., 2013. Anti-VCAM-1 and anti-E-selectin SAINT-O-Somes for selective delivery of siRNA into inflammation-activated primary endothelial cells. Mol. Pharm. 10 (8), 3033–3044.

Kowalski, P.S., Zwiers, P.J., Morselt, H.W., Kuldo, J.M., Leus, N.G., Ruiters, M.H., Molema, G., Kamps, J.A., 2014. Anti-VCAM-1 SAINT-O-Somes enable endothelial-specific delivery of siRNA and downregulation of inflammatory genes in activated endothelium in vivo. J. Control. Release 176, 64–75.

Lammers, T., Kiessling, F., Hennink, W.E., Storm, G., 2010. Nanotheranostics and image-guided drug delivery: current concepts and future directions. Mol. Pharm. 7 (6), 1899–1912.

Laquintana, V., Denora, N., Lopalco, A., Lopedota, A., Cutrignelli, A., Lasorsa, F.M., Agostino, G., Franco, M., 2014. Translocator protein ligand-PLGA conjugated nanoparticles for 5 fluorouracil delivery to glioma cancer cells. Mol. Pharm. 1 (3), 859–871.

Liang, M., Lv, J., Chu, H., et al., 2014. Vertical inhibition of PI3K/Akt/mTOR signaling demonstrates in vitro and in vivo anti-fibrotic activity. Dermatol. Sci. 76 (2), 104–111.
Liu, P., Cheng, H., Roberts, T.M., Zhao, J.J., 2009a. Targeting the phosphoinositide 3-kinase (PI3K) pathway in cancer. Nat. Rev. Drug Discov. 8, 627–644.
Liu, T.J., Koul, D., LaFortune, T., et al., 2009b. NVP-BEZ235, a novel dual phosphatidylinositol3-kinase/mammalian target of rapamycin inhibitor, elicits multifaceted antitumor activities in human gliomas. Mol. Cancer Theranostics 8 (8), 2204–2210.
Maeshima, Y., Makino, H., 2010. Angiogenesis and chronic kidney disease. Fibrogenesis Tissue Repair 3 (13), 1–17.
Maira, S.M., Stauffer, F., Brueggen, J., et al., 2008. Identification and characterization of NVP-BEZ235, a new orally available dual phosphatidylinositol 3-kinase/mammalian target of rapamycin inhibitor with potent in vivo antitumor activity. Mol. Cancer Ther. 7 (7), 1851–1863.
McCall, R.L., Sirianni, R.W., 2013. PLGA nanoparticles formed by single- or double-emulsion with vitamin E-TPGS. J. Vis. Exp. 82, 1–8.
Oliveira, S., Schiffelers, R.M., van der Veeken, J., van der Meel, R., Vongpromek, R., van Bergen En Henegouwen, P.M., Storm, G., Roovers, R.C., 2010. Downregulation of EGFR by a novel multivalent nanobody-liposome platform. J. Control. Release 145 (2), 165–175.
Pober, J.S., Sessa, W.C., 2007. Evolving functions of endothelial cells in inflammation. Nat. Rev. Immunol. 7, 803–815.
Polivka Jr., J., Janku, F., 2014. Molecular targets of cancer therapy in the PI3K/AKT/mTOR pathway. Pharmacol. Ther. 142, 164–175.
Pollock, C.B., Shirasawa, S., Sasazuki, T., Kolch, W., Dhillon, A.S., 2005. Oncogenic K-RAS is required to maintain changes in cytoskeletal organization, adhesion, and motility in colon cancer cells. Cancer Res. 65, 1244–1250.
Saha, B., Evers, T.H., Prins, M.W., 2014. How antibody surface coverage on nanoparticles determines the activity and kinetics of antigen capturing for biosensing. Anal. Chem. 86 (16), 8158–8166.
Samadi, N., van Steenbergen, M.J., van den Dikkenberg, J.B., Vermonden, T., van Nostrum, C.F., Amidi, M., Hennink, W.E., 2014. Nanoparticles based on a hydrophilic polyester with a sheddable PEG coating for protein delivery. Pharm. Res. 31 (10), 2593–2604.
Shortt, J., Martin, B.P., Newbold, A., Hannan, K.M., Devlin, J.R., Baker, A.J., Ralli, R., Cullinane, C., Schmitt, C.A., Reimann, M., Hall, M.N., Wall, M., Hannan, R.D., Pearson, R.B., McArthur, G.A., Johnstone, R.W., 2013. Combined inhibition of PI3K-related DNA damage response kinases and mTORC1 induces apoptosis in MYC-driven B-cell lymphomas. Blood 121 (15), 2964–2974.
Siepmann, J., Peppas, N.A., 2011. Higuchi equation: derivation, applications, use and misuse. Int. J. Pharm. 418 (1), 6–12.
Siepmann, J., Siepmann, F., 2012. Modeling of diffusion controlled drug delivery. J. Control. Release 161 (2), 351–362.
Spragg, D.D., Alford, D.R., Greferath, R., Larsen, C.E., Lee, K.D., Gurtner, G.C., Cybulsky, M.I., Tosi, P.F., Nicolau, C., Gimbrone Jr., M.A., 1997. Immunotargeting of liposomes to activated vascular endothelial cells: a strategy for siteselective delivery in the cardiovascular system. Proc. Natl. Acad. Sci. U. S. A. 94 (16), 8795–8800.
Sprague, A.H., Khalil, R.A., 2009. Inflammatory cytokines in vascular dysfunction and vascular disease. Biochem. Pharmacol. 78 (6), 539–552.
Tolias, K.F., Cantley, L.C., Carpenter, C.L., 1995. Rho family GTPases bind to phosphoinositide kinases. J. Biol. Chem. 270, 17656–17659.
Van den Mooter, G., Wuyts, M., Blaton, N., Busson, R., Grobet, P., Augustijns, P., Kinget, R., 2001. Physical stabilisation of amorphous ketoconazole in solid dispersions with polyvinylpyrrolidone K25. Eur. J. Pharm. Sci. 12 (3), 261–269.
Van der Meel, R., Vehmeijer, L.J., Kok, R.J., Storm, G., van Gaal, E.V., 2013. Ligand-targeted particulate nanomedicines undergoing clinical evaluation: current status. Adv. Drug Deliv. Rev. 65 (10), 1284–1298.
Vial, E., Sahai, E., Marshall, C.J., 2003. ERK-MAPK signaling coordinately regulates activity of Rac1 and RhoA for tumor cell motility. Cancer Cell. 4, 67–79.
Visweswaran, G.R., Gholizadeh, S., Ruiters, M.H., Molema, G., Kok, R.J., Kamps, J.A., 2015. Targeting rapamycin to podocytes using a vascular cell adhesion molecule-1 (VCAM-1)-Harnessed SAINT-Based lipid carrier system. PLoS One 10 (9), e0138870.
Wiechelman, K.J., Braun, R.D., Fitzpatrick, J.D., 1988. Investigation of the bicinchoninic acid protein assay: identification of the groups responsible for color formation. Anal. Biochem. 175, 231–237.
Williford, J.M., Ren, Y., et al., 2014. Shape transformation following reduction-sensitive PEG cleavage of polymer/DNA nanoparticles. J. Mater. Chem. B 2, 8106–8109.
Zhang, L., Gu, F.X., Chan, J.M., et al., 2008. Nanoparticles in medicine: therapeutic applications and developments. Clin. Pharmacol. Ther. 83 (5), 761–769.
Zhang, K., Tang, X., Zhang, J., Lu, W., Lin, X., et al., 2014. PEG-PLGA copolymers: their structure and structure-influenced drug delivery applications. J. Control. Release 183, 77–86.
Zweers, M.L., Engbers, G.H., Grijpma, D.W., Feijen, J., 2004. In vitro degradation of nanoparticles prepared from polymers based on DL-lactide: glycolide and poly (ethylene oxide). J. Control. Release 100 (3), 347–356.